Inter-comparison of relative stopping power estimation models for proton therapy

SHORT TITLE

Computing the proton relative stopping power

AUTHORS

P J Doolan[1*], Charles-Antoine Collins-Fekete[2,3], Marta F Dias[2,4], Thomas A. Ruggieri[2], Derek D'Souza[1], Joao Seco[2,5]

[1]Department of Radiotherapy Physics, University College London Hospital, London, U.K.

[2]Department of Radiation Oncology, Massachusetts General Hospital, Boston, MA, U.S.A.

[3]Departement de physique, de genie physique et d'optique et Centre de recherche sur le cancer, Universite Laval, Quebec

[4]Dipartamento di Elettronica, Informazione e Bioingegneria - DEIB, Politecnico di Milano, Italy

[5]Department of Medical Physics in Radiooncology, DKFZ German Cancer Research Center and Department of Physics and Astronomy, University of Heidelberg

[*]Corresponding author: paul.doolan@uclh.nhs.uk

ABSTRACT

Theoretical stopping power values were inter-compared for the Bichsel, Janni, ICRU and Schneider relative stopping power (RSP) estimation models, for a variety of tissues and tissue substitute materials taken from the literature. The RSPs of eleven plastic tissue substitutes were measured using Bragg peak shift measurements in water in order to establish a gold standard of RSP values specific to our centre's proton beam characteristics. The theoretical tissue substitute RSP values were computed based on literature compositions to assess the four different computation approaches. The Bichsel/Janni/ICRU approaches led to mean errors in the RSP of -0.1/+0.7/-0.8%, respectively. Errors when using the Schneider approach, with I-values from the Bichsel, Janni and ICRU sources, followed the same pattern but were generally larger. Following this, the mean elemental ionisation energies were optimized until the differences between theoretical RSP values matched measurements.

Failing to use optimized I-values when applying the Schneider technique to 72 human tissues could introduce errors in the RSP of up to -1.7/+1.1/-0.4% when using Bichsel/Janni/ICRU I-values, respectively. As such, it may be necessary to introduce an additional step in the current stoichiometric calibration procedure in which tissue insert RSPs are measured in a proton beam. Elemental I-values can then optimized to match these measurements, reducing the uncertainty when calculating human tissue RSPs.

1. Introduction and background

The characteristics of proton therapy beams, with a low entrance dose and sharp rise in dose at the end of the beam's range, gives them a distinct advantage over conventional photon therapy. The position of maximum dose (known as the Bragg peak) is dependent on the initial proton energy and can be carefully tuned to spare critical organs beyond the end of the range, provided the materials within the patient are known. Proton treatment planning requires knowledge of how the protons will be attenuated within the patient; information that is provided by a three-dimensional map of the patient's stopping powers relative to water (known as relative stopping powers, RSPs). Proton computed tomography (CT) scanners would provide such a dataset, however there are currently no clinical systems despite great research interest over many years (Cormack 1963, Hanson *et al* 1981, Schneider and Pedroni 1995, Zygmanski and Gall 2000, Sadrozinski 2003, Schulte *et al* 2004, 2005, Talamonti *et al* 2010, Hurley *et al* 2012, Testa *et al* 2013, Esposito *et al* 2015). Suggestions have been made to calibrate X-ray CT datasets using proton radiographic images (Schneider *et al* 2005, Doolan *et al* 2015), however this work remains in a preliminary stage.

The current clinical solution to generate this dataset is to convert the patient's X-ray CT from Hounsfield units (HU) into RSPs using a calibration curve (known as a HU-RSP calibration curve). This HU-RSP calibration curve is subject to a number of uncertainties. The X-ray CT can be affected by patient size and beam hardening (Schaffner and Pedroni 1998), changes in the photon energy spectra (Qi *et al* 2006), drifts of the scanner with time (Yang *et al* 2012), noise (Chvetsov and Paige

2010), detector sensitivity and the choice of reconstruction algorithm (Kanematsu *et al* 2003) and artefacts from metallic objects (Verburg and Seco 2012). The accuracy of the RSP calculation is dependent on the uncertainty of the real tissue composition (Woodard and White 1986, White *et al* 1987, ICRU 1989), deviations of the patient from these literature compositions (Schneider *et al* 2005, Yang *et al* 2012, Doolan *et al* 2015) and uncertainties in the mean ionisation energies (henceforth referred to as 'I-value') of tissue and water (Andreo 2009, Yang *et al* 2012). Additionally, there does not exist a perfect one-to-one correspondence between CT numbers and RSP of human tissues (Yang *et al* 2012). The uncertainty in the HU-RSP calibration curve leads to an uncertainty of where the protons will stop in the patient, known as 'range uncertainty'. In clinical practice a margin of 2.5-3.5% of the beam range is added to account for the proton beam range uncertainty, with this conversion from HU to RSP contributing ±0.5% to the uncertainty and uncertainties in the tissue I-values contributing a further ±1.5% (both based on 1.5 standard deviations) (Paganetti 2012).

1.1. Stoichiometric calibration

The stoichiometric approach, first proposed by Schneider *et al* (1996), is the most widely used method for producing the HU-RSP calibration curve (Taylor 2015b). The process consists of four main steps:

1. Image tissue-substitute materials with a known chemical composition.
2. Parameterise the response of the CT as a function of the material's chemical composition. As described in Schneider *et al* (2000) the mean attenuation coefficient $\overline{\mu}$ for the range of diagnostic X-ray energies and the elements contained in human tissues is described in good approximation as,

$$\overline{\mu} = \rho N_A (Z\overline{K}^{\mathrm{KN}} + Z^{2.86}\overline{K}^{\mathrm{sca}} + Z^{4.62}\overline{K}^{\mathrm{ph}}) \quad (1)$$

where ρ is the mass density; N_A is Avagadro's constant (6.022×10^{23}); Z is the effective atomic number (calculated using the fraction by weight of the individual elements for compounds); $\overline{K}^{\mathrm{KN}}$ is the Klein-Nishina coefficient; $\overline{K}^{\mathrm{sca}}$ accounts for coherent scattering and

the binding correction for incoherent scattering; and $\overline{K}^{\mathrm{ph}}$ accounts for photoelectric absorption. The values

$$k_1 \equiv \frac{\overline{K}^{\mathrm{sca}}}{\overline{K}^{\mathrm{KN}}} \qquad k_2 \equiv \frac{\overline{K}^{\mathrm{ph}}}{\overline{K}^{\mathrm{KN}}} \tag{2}$$

are CT scanner dependent and are determined experimentally through the scanning of tissue equivalent plastics of known chemical composition. The values of k_1 and k_2 are determined by conducting a least square fit to the measured CT numbers, as described in detail in Schneider *et al* (2000).

3. Calculate the CT numbers of human biological tissues. In an ideal scenario these would not require calculation, but rather would be measured directly in the CT scanner. However, this is rarely practical. Even if real tissues could be readily handled, it would still require the separate scanning of individual tissues (to avoid problems such as beam hardening). Therefore, the CT numbers for real biological tissues are theoretically predicted using equation 1, together with the fitted constants. Chemical compositions and effective densities are taken from literature such as Woodard and White (1986), White *et al* (1987) and ICRU (1989).
4. Calculate the RSPs of human biological tissues. As with step 3, in an ideal scenario these would be measured directly with a proton beam, but again this is not practical. Therefore, these values have to be theoretically calculated using the same chemical compositions from literature (Woodard and White 1986, White *et al* 1987, ICRU 1989). The absolute stopping power depends on the energy of the particle, but the RSP is almost independent of β (particle velocity in units of the velocity of light) for the range of particle energies relevant to radiation therapy (Hanson *et al* 1981, Arbor *et al* 2015). As such, the RSP is a much more useful quantity for proton therapy treatment planning, where the beam energy varies with depth in the patient.

Other stoichiometric calibration procedures also exist, such as the de Kock (2003) and Kanematsu *et al* (2003) approaches, offering potential advantages. For instance, if there are high density materials causing beam hardening artefacts, and if these are not compensated by the reconstruction algorithm there will be a varying X-ray energy spectrum throughout the object. In such cases, a non-linear model should be used to compute the CT numbers, such as that used in the de Kock (2003) routine. An advantage of the polybinary tissue model suggested by Kanematsu *et al* (2003) is that it requires the scanning of far fewer materials (four), with little compromise on the accuracy. For the purposes of this work, only the Schneider stoichiometric calibration procedure is considered.

1.2. Use of the stoichiometric calibration in clinical practice

As stated at the start of Section 1.1, the stoichiometric calibration is the most common approach for producing the HU-RSP calibration curve. In 2015, the Imaging and Radiation Oncology Core (IROC) Houston conducted proton beam validation tests on 15 proton centres in the United States, for clinical trials purposes (Taylor 2015b). According to the authors (Taylor 2015a), ten of these centres produced their calibration curves with the stoichiometric method, four used measurements and one institution used an in-house Monte Carlo calculation. Of the ten using a stoichiometric calibration, four used the Schneider *et al* (1996) calibration, five used a modified version implemented in the program by de Kock *et al* (2003) and one used the modified version suggested by Kanematsu *et al* (2003).

Across the 15 institutions, both the CIRS and Gammex phantoms were used, as well as pork and bone animal tissue. Ainsley and Yeager (2014) showed that the specific choice of phantom has no impact on the uncertainty in the calibration curve. According to IROC Houston (Taylor 2015a), the average number of human tissues computed is 40: the de Kock program computes 64 human tissues, while the average for the other institutions using the stoichiometric method was 12 tissues. Information about the source from which the I-values were obtained was not provided.

1.3. Theoretical calculation of the RSP

Most previous works, such as Yang *et al* (2012), have looked at the errors introduced by the complete stoichiometric calibration procedure. In this work we look specifically at step four of the stoichiometric calibration procedure; the calculation of the theoretical RSP. The Bethe-Bloch formula is used to compute the stopping power of tissue, however there exists in literature a number of different approaches with different correction terms and sets of I-values. We are aware of four different approaches:

i. The first proposal was given by Bichsel (1972), with the stopping power S_B given by:

$$S_B = \rho \frac{4\pi e^4}{m_e c^2 u \beta^2} z^2 \frac{Z}{A} \left\{ \ln\left[\frac{2m_e c^2 \beta^2}{(1-\beta^2)} \right] - \beta^2 - \ln I_t - \frac{C}{Z} - \frac{\delta}{2} \right\} \quad (3)$$

where ρ is the mass density; e is the electron charge; $m_e c^2$ is the rest mass energy of the electron; u is the atomic mass unit; z is the charge of the projectile (+1 for protons); Z and A are the atomic number and relative atomic mass of the target atom; $\beta = v/c$, the particle velocity in units of the velocity of light; I_t is the I-value of the tissue; C/Z is the shell correction; and $\delta/2$ is the density correction. The RSP can then be calculated by dividing by the stopping power of water over the same energy range. To allow for comparison with other equations, we can rewrite the formula of Bichsel (equation 2) as,

$$S_B = K \times B \quad (4)$$

where K is the term outside the brackets and B represents the terms inside the brackets (the letter B used to represent Bichsel).

ii. Using the above definitions, it is possible to write the stopping power as defined by Janni (1982) S_J as,

$$S_J = K \left\{ B - \frac{1}{2} \ln\left[1 + \frac{2m_e}{M\sqrt{(1-\beta^2)}} + \left(\frac{m_e}{M} \right)^2 \right] + \frac{\pi \alpha z \beta}{2} + \frac{z Z \alpha^3 F(\beta, Z)}{\beta^3} \right\} \quad (5)$$

where M is the proton rest mass and the second term in the square brackets forms part of the factor that accounts for the maximum kinetic energy that can be transferred to an unbound electron at rest; α is the fine structure constant, equal to 1/137.036; the second last term is important only relativistically; the final term is the Barkas correction, where the function

F(β,Z) is important only at low energies and is usually set to zero; and all other parameters are as defined previously. To allow comparison with the ICRU formula (see below), the formula of Janni (equation 4) can be rewritten as,

$$S_J = K\{B + J_1 + J_2 + J_3\} \tag{6}$$

where $J_{1,2,3}$ are the second, third and fourth terms inside the brackets of equation 4 (the letter *J* used to represent Janni).

iii. Using the previous definitions, the stopping power as defined by ICRU (1993) Report 49 can be written as,

$$S_I = K\left\{B + J_1 + \gamma J_3 - \left(\frac{z\alpha}{\beta}\right)^2 \sum_{n=1}^{\infty}\left[n\left(n^2 + \left(\frac{z\alpha}{\beta}\right)^2\right)\right]^{-1}\right\} \tag{7}$$

where γ comes from the use of the free-electron model and is approximately equal to $\sqrt{2}$; the final term in brackets is known as the Bloch correction; and all other parameters are as defined previously. In the ICRU Report, there are I-values for elements and for atomic constituents of compounds in the liquid and solid phase. Only the latter are considered in this work.

iv. The Bichsel, Janni and ICRU approaches above are all used to compute the absolute stopping power of tissue. In order to determine the relative stopping power of tissue, it is necessary to divide by the absolute stopping power of water over the same energy range. Alternatively, and more conveniently, the RSP can be approximated directly by ignoring many of the correction terms. To the best of the authors' knowledge, this was first proposed by Schneider *et al* (1996),

$$RSP = \rho_e^{rel}\frac{\ln[2m_e c^2\beta^2 / I_t(1-\beta^2)] - \beta^2}{\ln[2m_e c^2\beta^2 / I_w(1-\beta^2)] - \beta^2} \tag{8}$$

where ρ_e^{rel} is the volumetric electron density relative to water; I_t and I_w are the I-values of tissue and water respectively; and all other symbols are as defined previously. This approach is currently the most popular as it avoids use of the many small corrections that are difficult to compute and are assumed to be negligible for biological tissues (Ödén *et al* 2015).

1.4. Corrections and mean ionisation values

The different formulae described in Bichsel, Janni and ICRU (equations 3, 5 and 7, respectively) account for different effects. All formulae account for the shell and density corrections. The density effect is caused by the passing proton polarizing the surrounding atoms of the medium, perturbing the electron field and reducing the energy lost by the proton by up to 10%. The Janni and ICRU formulae (equations 5 and 7) have additional corrections: (i) a factor is included that accounts for the maximum kinetic energy that can be transferred to an unbound electron at rest; and (ii) the Barkas correction that accounts for the charge of the particle, in which slightly smaller stopping powers are experienced by negative particles compared to positive particles of the same mass and velocity. The ICRU formula also implements the Bloch correction, which accounts for instances when the projectile velocity is comparable to the velocities of the atomic electrons.

Ödén *et al* (2015) compared the use of the Schneider approximation of the RSP (equation 8), that does not include these correction terms, with the well-known SRIM software (www.srim.org), which accounts for the above corrections. They showed that these correction terms introduce discrepancies of less than 0.1% across 72 human tissues. However, the Bichsel, Janni and ICRU formulae all incorporate different corrections and as a result each source uses different I-values. This is also partly due to their date of publication and the data available to the authors at the time. In this work we show explicitly the impact of using the different literature approaches and their corresponding I-values.

These values, together with the computed values for our tissue substitutes and, importantly, water (I_w), are detailed in table 1. Tissue I-values I_t are computed using Bragg's additivity rule (Seltzer and Berger 1982, ICRU 1992),

$$\ln I_t = \left(\sum \frac{\omega_i Z_i}{A_i} \ln I_i \right) \left(\sum \frac{\omega_i Z_i}{A_i} \right)^{-1} \tag{9}$$

where I_i are individual elemental I-values; Z_i and A_i are the atomic number and atomic weight of the i[th] element and ω_i is its proportion by weight. The ICRU values are the mean excitation energies for atomic constituents of compounds (from tables 2.11 and 2.8 of ICRU Report 49); and their uncertainties are from table 2.8 in ICRU Report 49.

Element (Z) or material	I value [eV]		
	(Bichsel 1972) and (Bichsel and Hiraoka 1992)*	(Janni 1982)	(ICRU 1993)
H (1)	19.2	20.4	19.2 ± 0.4
C (6)	86.9*	73.8	81 ± 7
N (7)	80	97.8	82 ± 2
O (8)	95	115.7	106 ± 2
F (9)	119	124.8	112 ± 0
Na (11)	148	143.0	168.4 ± 0
Mg (12)	156	151.1	176.3 ± 0
Si (14)	176*	174.5	195.5 ± 3
P (15)	172	179.1	195.5 ± 0
S (16)	180	183.6	203.4 ± 0
Cl (17)	187	182.6	180 ± 0
K (19)	193	186.8	214.7 ± 0
Ca (20)	196	191.9	215.8 ± 8
Fe (26)	293*	278.2	323.2 ± 9
I (53)	510	515.2	535.6 ± 0
LN-300 Lung	74.4	71.0	73.9
LN-450 Lung	74.3	70.9	73.8
AP6 Adipose	68.6	64.3	66.6
Breast	70.0	65.9	68.2
CT Solid Water	71.9	68.2	70.4
Brain	65.5	61.4	63.5
Liver	71.8	68.2	70.3
IB3 Inner Bone	80.1	77.7	80.1
CB2 30% $CaCO_3$	80.6	78.5	80.7
CB2 50% $CaCO_3$	90.9	90.9	93.2
SB3 Cortical Bone	100.2	102.4	104.5

Water	79.7*	81.8	75.3

*Table 1: I-values of elements, tissue substitutes and water, calculated using the different sources.*Values from the more recent source.*

215

1.5. Aim of this work

It is clear that the stoichiometric calibration procedure is in widespread use. Although its implementation is not consistent between centres (the Schneider, de Kock and Kanematsu methods are all used), step four, the theoretical calculation of the RSP, is a necessary step for all those using a
220 stoichiometric calibration. In literature there currently exist a number of methods for this computation based on the Bethe-Bloch theory, with no clear consensus as to which approach introduces the lowest error in the calibration curve. The Bichsel, Janni and ICRU approaches involve calculating the absolute stopping power of tissue and dividing by the respective stopping power of water over the same energy range; while in the Schneider approach many of the corrections are neglected and the
225 RSP is approximated directly. Much work has investigated the impact of proton energy loss below 1 MeV (Liamsuwan *et al* 2011, 2015), but this work is specifically concerned with the assessment of the RSP models at energies that have a significant clinical impact on the proton range. Additionally, the impact of the I-value of water has been extensively investigated by Andreo (2009) and Yang *et al* (2012) and so is not revisited. In all theoretical calculations the I-value of water was set to the values
230 listed in table 1. The work is split into three parts:

1. *Absolute stopping power computation:* The first aim of this work is to investigate the error introduced if the RSP is calculated using the separate absolute stopping power formulae of Bichsel, Janni and ICRU and their respective I-values (i.e. Bichsel formula with Bichsel I-values etc.). Theoretical predictions of tissue substitutes are compared to measurements in a
235 proton beam.
2. *Schneider RSP computation:* Most centres use the Schneider formula (or the de Kock or Kanematsu approaches) because of its greater simplicity: RSP is directly approximated and it avoids the many corrections that can be difficult to compute. However it should be stressed

that this formula is not a derived theoretical method and in such a simplification there is not a corresponding set of I-values. As such, the second aim of this work is to compute the RSP errors in using each set of I-values (Bichsel, Janni and ICRU) with the Schneider approximation, compared to tissue substitute measurements in a proton beam.

3. *Potential solution:* No centres currently use the Bichsel, Janni or ICRU techniques for computing the absolute stopping power (Taylor 2015a), because the Schneider approach (and its variations) for computing the RSP are considerably simpler. However, as stated above, there are no suitable I-values for such an approximation. The final aim of this work is therefore to propose a method whereby the I-values are fitted to the measurements of the Gammex insert RSPs. These I-values are then used for theoretical human tissue RSP computations using the Schneider formulation, and comparisons are made with the values obtained when using the Bichsel, Janni and ICRU I-values.

2. Methods and Materials

2.1.Measurements

A selection of the tissue substitute materials of the Gammex RMI 467 phantom (Gammex Inc., Middleton, WI) were imaged using the standard arrangement suggested by the manual, with an X-ray CT at 140 kVp. Bone mineral B200 was excluded because it has a significant proportion of fluorine (16.7%) and none of the human body tissues contain fluorine. The physical characteristics of the 11 inserts can be found in table 2. Mass and electron densities relative to water, specific to this particular batch, were provided from the manufacturer (Gammex) and used in the computation. The mass densities were independently verified using mass (using an Acculab scale) and volume measurements (using Starett Co. micrometers), with a mean difference of +0.4% compared to the vendor's information. Individual insert compositions can be found in table 2, derived from vendor data.

Substitute	Mass density [g cm^{-3}]	Relative electron density	H 1	C 6	N 7	O 8	Mg 12	Si 14	P 15	Cl 17	Ca 20
LN-300 Lung	0.28	0.28	8.46	59.37	1.96	18.14	11.19	0.78	0.00	0.10	0.00

LN-450 Lung	0.47	0.46	8.47	59.56	1.97	18.11	11.21	0.58	0.00	0.10	0.00
AP6 Adipose	0.94	0.93	9.06	72.29	2.25	16.27	0.00	0.00	0.00	0.13	0.00
Breast	0.98	0.96	8.59	70.10	2.33	17.90	0.00	0.00	0.00	0.13	0.95
CT Solid Water	1.02	0.99	8.00	67.29	2.39	19.89	0.00	0.00	0.00	0.14	2.31
Brain	1.05	1.05	10.83	72.54	1.69	14.86	0.00	0.00	0.00	0.08	0.00
Liver	1.09	1.06	8.06	67.01	2.47	20.01	0.00	0.00	0.00	0.14	2.31
IB3 Inner Bone	1.14	1.09	6.67	55.65	1.96	23.52	0.00	0.00	3.23	0.11	8.86
CB2 30% $CaCO_3$	1.33	1.28	6.68	53.47	2.12	25.61	0.00	0.00	0.00	0.11	12.01
CB2 50% $CaCO_3$	1.56	1.47	4.77	41.62	1.52	31.99	0.00	0.00	0.00	0.08	20.02
SB3 Cortical Bone	1.82	1.70	3.41	31.41	1.84	36.50	0.00	0.00	0.00	0.04	26.81
Water	1.00	1.00	11.20	0.00	0.00	88.80	0.00	0.00	0.00	0.00	0.00

Table 2: Physics characteristics and elemental compositions for the Gammex 467 phantom.

The insert RSPs were measured directly using a Bragg peak shift measurement. Similar measurements have been used in previous works (Zhang *et al* 2010, Sánchez-Parcerisa *et al* 2012). This involved setting a consistent proton beam range (159 MeV, distal R80 = 17.3 cm in water) and measuring the shift in the Bragg peak position, with and without an insert in the beam path. A pencil proton beam was generated using a brass aperture equal to the diameter of the inserts (28.6 mm), as shown in figure 1. The inserts were inserted into the aperture and the Bragg peak position was measured using two instruments: (i) a Markus ionisation chamber, positioned within a tank of water (together with a reference chamber at the entrance of the tank). The Markus chamber was stepped through positions 1 mm apart and interpolation between these measurements provides a sub-millimetre range resolution of the Bragg peak. (ii) The Bragg peak shift was also measured with the Zebra (IBA Dosimetry, Belgium), a commercial stack of parallel plate ionisation chambers. Successive plates are 2 mm apart, however the range resolution of the Bragg peak is ±0.5 mm with interpolation (Ion Beam Applications, Louvain-la-Neuve). The ionisation chamber and water tank combination is considered a more accurate absolute measurement, however it can be susceptible to setup errors of up to 1 mm. The relative range measurement offered by the Zebra can be acquired faster and is robust against the type

of setup errors that can occur with the water tank; however the range resolution is intrinsically limited. As such, the mean of the two measurements was used to compute the insert RSP.

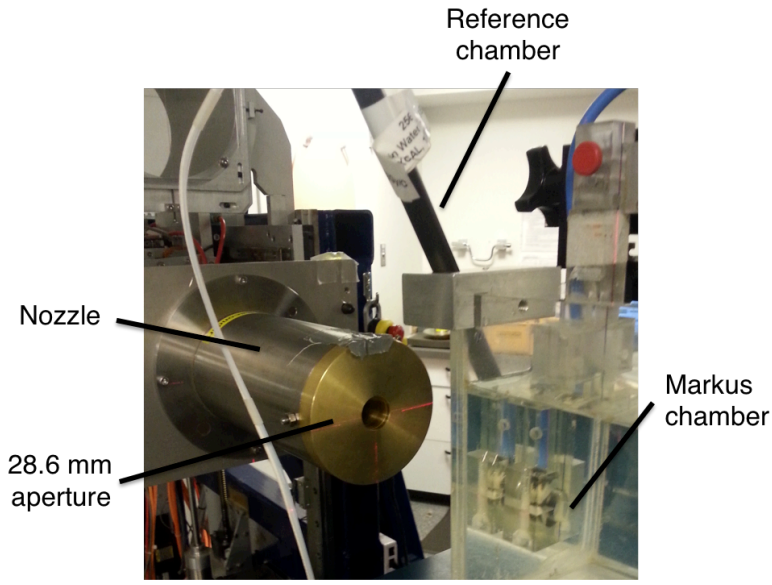

Figure 1. Photograph showing the set up for measurements. Inserts were inserted into the aperture and Bragg peak shifts were measured in the water tank.

Insert thicknesses were measured using a calibrated set of callipers to a precision of ±0.05 mm. The ratio of the water equivalent shift (the shift with and without the insert) and the thickness of the insert allowed for computation of the insert RSP. The water equivalent shifts of both the distal 80% (known as R80 (Gottschalk 2003)) and distal 90% (known as R90 (Zhang *et al* 2010)) were determined to investigate the sensitivity of the RSP to the range determination method.

2.2. Absolute stopping power calculation

Using estimates of the chemical composition from the vendor, the absolute stopping powers for these tissue inserts were calculated using the different formulae and their listed I-values: (i) Bichsel (1972), equation 3; (ii) Janni (1982), equation 5; and (iii) ICRU (1993), equation 7, with compound I-values (a total of three computations). The RSP for each tissue was then determined by dividing by the respective stopping power of water (i.e. calculated using the same source) and taking the average over the energy range relevant to proton therapy and proton imaging (10-330 MeV). These calibration

curves will be referred to as the 'Bichsel', 'Janni', 'ICRU' calibration curves, or collectively as the 'absolute stopping power curves', for the remainder of this work.

2.3. Schneider RSP computation

The RSP of each Gammex tissue substitute was approximated using the Schneider approximation (equation 8), with I-values from each of the three sources (Bichsel (1972), Janni (1982) and ICRU (1993)). These three calibration curves will be referred to collectively as the 'Schneider calibration curves' for the remainder of this work.

2.4. Fitting I-values to measurement

Most centres use the Schneider approximation for the RSP that does not account for corrections (Section 1.4), together with a set of I-values that is intended to be used with corrections. In an attempt to offer a solution to this discrepancy, an approach was developed in which elemental I-values were modified using an iterative optimization process, until the theoretical RSP computations matched the experimental RSP results for the tissue substitutes. The optimizer utilises Matlab's built-in Nelder–Mead optimization function, 'fminsearch'. Such optimizers are robust to local minima and do not require an equation to be provided for the derivative of the cost function (Lagarias *et al* 1998), making their implementation simple.

The ICRU elemental I-values were utilised as the starting point, as the ICRU publication is the most recent and likely the most often used by centres. These elemental I-values were varied during the optimization process, until the difference between the theoretical tissue substitute RSP computation and the measured tissue substitute RSP was minimal. The cost function Δ to describe this difference was defined as the root mean square error, also accounting for the uncertainty in the measurement,

$$\Delta = \frac{1}{n}\sqrt{\frac{\sum_i \left(RSP_c^i - RSP_i^m\right)^2}{\sum_i \left(RSP_m^i\right)^2}\ \frac{1}{\left(Err_m^i\right)^2}}\ , \tag{10}$$

where n is the number of tissue substitutes; RSP_c^i and RSP_m^i are the computed and measured RSP values for the tissue substitute i; and Err_m^i is the uncertainty in the measurement for tissue substitute i. To avoid nonphysical results, appropriate conditioning was required. The upper and lower bounds for each elemental I-value were taken from the uncertainties in ICRU Report 49 (it should be noted that under this restriction only 7 of the 15 elements were allowed to vary). Full details of the optimization process are detailed in table 3.

Variable	Details	Value(s) used
MaxFunEvals	Maximum number of evaluations of the cost function (where n is the number of variables = 7)	1000 x n
TolFun	Absolute tolerance on function value	1×10^{-4}
Starting condition	ICRU elemental I-values	Nominal I-values below
Constraints	Uncertainties in elemental I-values given by ICRU (1993)	H(1) = 19.2 ± 0.4 eV C(6) = 81 ± 7 eV N(7) = 82 ± 2 eV O(8) = 106 ± 2 eV F(9) = 112 ± 0 eV Na(11) = 168.4 ± 0 eV Mg(12) = 176.3 ± 0 eV Si(14) = 195.5 ± 3 eV P(15) = 195.5 ± 0 eV S(16) = 203.4 ± 0 eV Cl(17) = 180 ± 0 eV K(19) = 214.7 ± 0 eV Ca(20) = 215.8 ± 8 eV Fe(26) = 323.2 ± 9 eV I(53) = 535.6 ± 0 eV
RSP computation	Approach used to compute the RSP	Schneider (equation 8)

Table 3: Input variables for the optimization.

3. Results

3.1. Measurements

Measured CT values and Bragg peak shift measurement data for the Gammex inserts is detailed in table 4. The R80 and R90 shift values are each an average of the two measurements, with a Markus chamber in a water tank and with the Zebra. The mean difference between the R80 and R90 shifts was only 0.2%, suggesting our measurements were largely unaffected by the potential broadening of the beam through the insert. Errors in the RSP are computed based on the propagation of the standard

deviation of the two measurements (Markus and Zebra) and the precision of the thickness measurement.

Insert material	CT number [HU]	R80 shift* [mm]	R90 shift* [mm]	Thickness [mm]	RSP (R80)	RSP (R90)
LN-300 Lung	-727.9	-20.2±0.1	-20.3±0.2	72.2±0.1	0.280±0.002	0.281±0.003
LN-450 Lung	-522.6	-33.9±0.0	-33.9±0.2	71.6±0.1	0.473±0.001	0.474±0.003
Adipose	-83.8	-66.5±0.0	-66.4±0.3	70.3±0.1	0.946±0.001	0.945±0.005
Breast	-41.9	-68.7±0.0	-68.6±0.3	70.5±0.1	0.974±0.001	0.973±0.005
CT Solid Water	1.0	-70.7±0.1	-70.5±0.5	70.3±0.1	1.005±0.002	1.003±0.007
Brain	25.0	-75.1±0.1	-75.0±0.4	70.4±0.1	1.067±0.003	1.065±0.006
Liver	83.7	-75.9±0.2	-74.7±0.2	70.2±0.1	1.080±0.003	1.064±0.024
Inner Bone	204.0	-76.8±0.4	-76.8±0.9	70.3±0.1	1.094±0.006	1.093±0.014
CB2 30% $CaCO_3$	455.8	-88.4±0.7	-88.3±0.1	70.1±0.1	1.260±0.010	1.259±0.017
CB2 50% $CaCO_3$	798.0	-100.5±0.4	-100.3±0.1	70.2±0.1	1.433±0.006	1.430±0.010
SB3 Cortical Bone	1203.1	-113.7±0.4	-113.7±0.1	70.2±0.1	1.620±0.006	1.620±0.014

*Table 4. Measurement data for the Gammex RMI 467 tissue substitute inserts. *Shift in R80 and R90 positions with respect to measurement without insert (average values across the two measurements, with Markus and Zebra).*

Using the measured CT values of the tissue substitutes, table 4, the response of the CT was parameterised as a function of chemical composition. Using equations 1 and 2 and estimates of the chemical composition from the vendor, the constants were found to be $k_1 = 3.30330 \times 10^{-5}$ and $k_2 = 1.86869 \times 10^{-4}$, with an $r^2 = 0.998$. These constants, together with composition data from literature (Woodard and White 1986, White *et al* 1987, ICRU 1993), were then used to determine the theoretical CT values for human tissues.

3.2. Absolute stopping power calculation

The theoretical values of RSP for the tissue substitutes, calculated using the Bichsel, Janni and ICRU stopping power formulae (equations 3, 5, 7) and averaged over the energy range 10-330 MeV, are detailed in table 5. The Bichsel and ICRU approaches generally underestimate, while Janni

overestimates. Averaging over all inserts, all three approaches demonstrate a good match to measurements.

Material	Measured	Bichsel		Janni		ICRU	
		RSP	Err (%)	RSP	Err (%)	RSP	Err (%)
LN-300 Lung	0.280	0.275	-1.74	0.278	-0.82	0.273	-2.37
LN-450 Lung	0.473	0.462	-2.33	0.466	-1.42	0.459	-2.96
Adipose	0.946	0.943	-0.34	0.954	+0.81	0.939	-0.69
Breast	0.974	0.975	+0.10	0.985	+1.19	0.971	-0.30
CT Solid Water	1.005	1.001	-0.42	1.011	+0.58	0.996	-0.88
Brain	1.067	1.077	+0.92	1.089	+2.10	1.073	+0.58
Liver	1.080	1.072	-0.70	1.083	+0.28	1.067	-1.16
Inner Bone	1.094	1.092	-0.16	1.100	+0.57	1.084	-0.89
CB2 30% $CaCO_3$	1.260	1.275	+1.21	1.284	+1.88	1.266	+0.45
CB2 50% $CaCO_3$	1.433	1.444	+0.74	1.448	+1.08	1.429	-0.31
Cortical Bone	1.620	1.619	+1.47	1.644	+1.50	1.623	+0.15
		RMSE*	+1.14		+1.24		+1.30
		Mean	-0.12		+0.71		-0.76
		Max^	-2.33		+2.10		-2.96

*Table 5. Relative stopping powers (RSP) for the Gammex tissue substitutes, calculated using the individual source formulae. The percentage error ('Err') with respect to the measurement is listed. *Root-mean-square-error. ^Maximum error (in either positive or negative direction).*

3.3. Schneider RSP computation

Using the I-values from the three sources (Bichsel, Janni and ICRU), but with the Schneider approximation for the RSP, equation 8, gives the theoretical values for RSP as detailed in table 6. It can be seen that this theoretical calculation of RSP, step four of the stoichiometric procedure, follows the same pattern as the results in table 5: a systematic underestimation in the Bichsel and ICRU approaches and an overestimation in the Janni scheme. In this instance, using the ICRU I-values results in the lowest error. The errors are generally larger than the absolute stopping power computations, which is not surprising as the individual sets of I-values account for correction terms that are not present in the Schneider approach.

Material	Measured	Bichsel		Janni		ICRU	
		RSP	Err (%)	RSP	Err (%)	RSP	Err (%)
LN-300 Lung	0.280	0.274	-2.30	0.281	+0.23	0.277	-1.21
LN-450 Lung	0.473	0.458	-3.17	0.470	-0.66	0.463	-2.09
Adipose	0.946	0.927	-2.05	0.953	+0.70	0.940	-0.69
Breast	0.974	0.957	-1.71	0.984	+0.98	0.970	-0.39
CT Solid Water	1.005	0.983	-2.17	1.010	+0.43	0.999	-0.91
Brain	1.067	1.056	-1.00	1.086	+1.78	1.071	+0.39
Liver	1.080	1.053	-2.50	1.081	+0.09	1.067	-1.25
Inner Bone	1.094	1.075	-1.75	1.101	+0.61	1.086	-0.73
CB2 30% $CaCO_3$	1.260	1.254	-0.49	1.283	+1.83	1.267	+0.51
CB2 50% $CaCO_3$	1.433	1.423	-0.73	1.451	+1.28	1.433	0.00
Cortical Bone	1.620	1.621	+0.06	1.649	+1.82	1.629	+0.57
		RMSE*	+1.86		+1.13		+0.96
		Mean	-1.62		+0.83		-0.53
		Max^	-3.17		+1.83		-2.09

*Table 6. Relative stopping powers (RSP) for the Gammex tissue substitutes, calculated using the Schneider approximation for the RSP, equation 8, but with the I-values of the different sources. The percentage error ('Err') with respect to the measurement is listed. *Root-mean-square-error. ^Maximum error (in either positive or negative direction).*

2.4. Fitting I-values to measurement

As shown in the previous sections, all the current approaches have discrepancies from the measured values. Optimizing the elemental I-values (see values in table 7), significantly improved the estimates of tissue substitute RSP, as detailed in table 8. The cost function RMSE decreased from 0.96% to 0.76%, while the mean error across the tissue substitutes decreased from -0.53% to +0.11%. The RSP approximation improved in 7 out of 11 inserts.

	I value (eV)	
Material	ICRU	Optimized
H (1)	19.2 ± 0.4	18.8
C (6)	81 ± 7	74

N (7)	82 ± 2	80
O (8)	106 ± 2	104
F (9)	112 ± 0	112
Na (11)	168.4 ± 0	168.4
Mg (12)	176.3 ± 0	176.3
Si (14)	195.5 ± 3	192.5
P (15)	195.5 ± 0	195.5
S (16)	203.4 ± 0	203.4
Cl (17)	180 ± 0	180
K (19)	214.7 ± 0	214.7
Ca (20)	215.8 ± 8	223.8
Fe (26)	323.2 ± 9	331.7
I (53)	535.6 ± 0	535.6

Table 7. Original and optimized elemental I-values.

Material	Measured	ICRU		Optimized	
		RSP	Err (%)	RSP	Err (%)
LN-300 Lung	0.280	0.277	-1.21	0.279	-0.55
LN-450 Lung	0.473	0.463	-2.09	0.466	-1.43
Adipose	0.946	0.940	-0.69	0.947	+0.09
Breast	0.974	0.970	-0.39	0.978	+0.37
CT Solid Water	1.005	0.999	-0.91	1.003	-0.18
Brain	1.067	1.071	+0.39	1.079	+1.15
Liver	1.080	1.067	-1.25	1.074	-0.52
Inner Bone	1.094	1.086	-0.73	1.093	-0.12
CB2 30% $CaCO_3$	1.260	1.267	+0.51	1.274	+1.10
CB2 50% $CaCO_3$	1.433	1.433	0.00	1.439	+0.45
Cortical Bone	1.620	1.629	+0.57	1.635	+0.90
	RMSE*		+0.96		+0.76
	Mean		-0.53		+0.11
	Max^		-2.09		-1.43

Table 8. The impact of optimizing the elemental I-values on the tissue substitute RSPs.

390

Figure 2 shows the optimized elemental I-values in comparison with the Bichsel, Janni and previous (unoptimized) ICRU results. Altering the elemental I-values leads to a variation in the tissue I-values.

Using compositions from literature (Woodard and White 1982, White *et al* 1987, ICRU 1989), the variation in I-value across 72 human tissues is shown in figure 3.

395

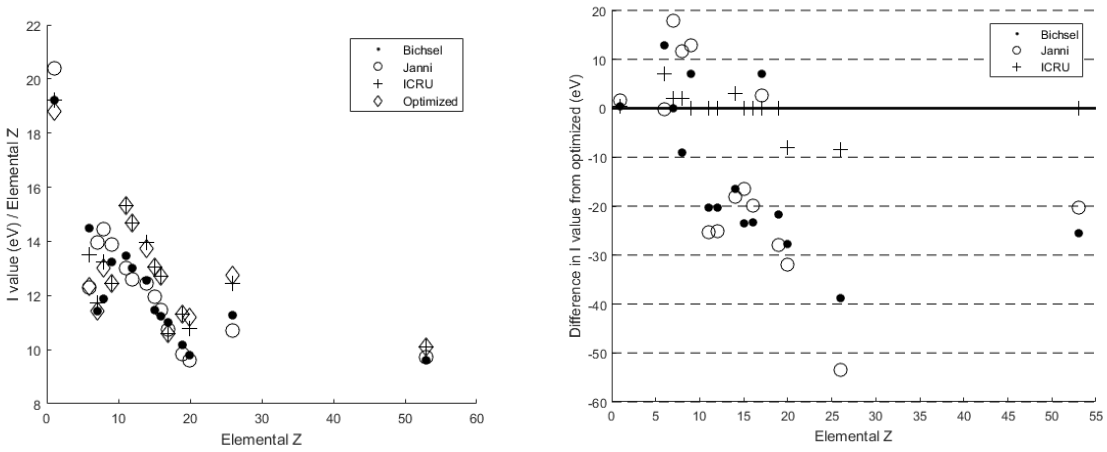

Figure 2. Optimized elemental I-values in comparison with literature values.

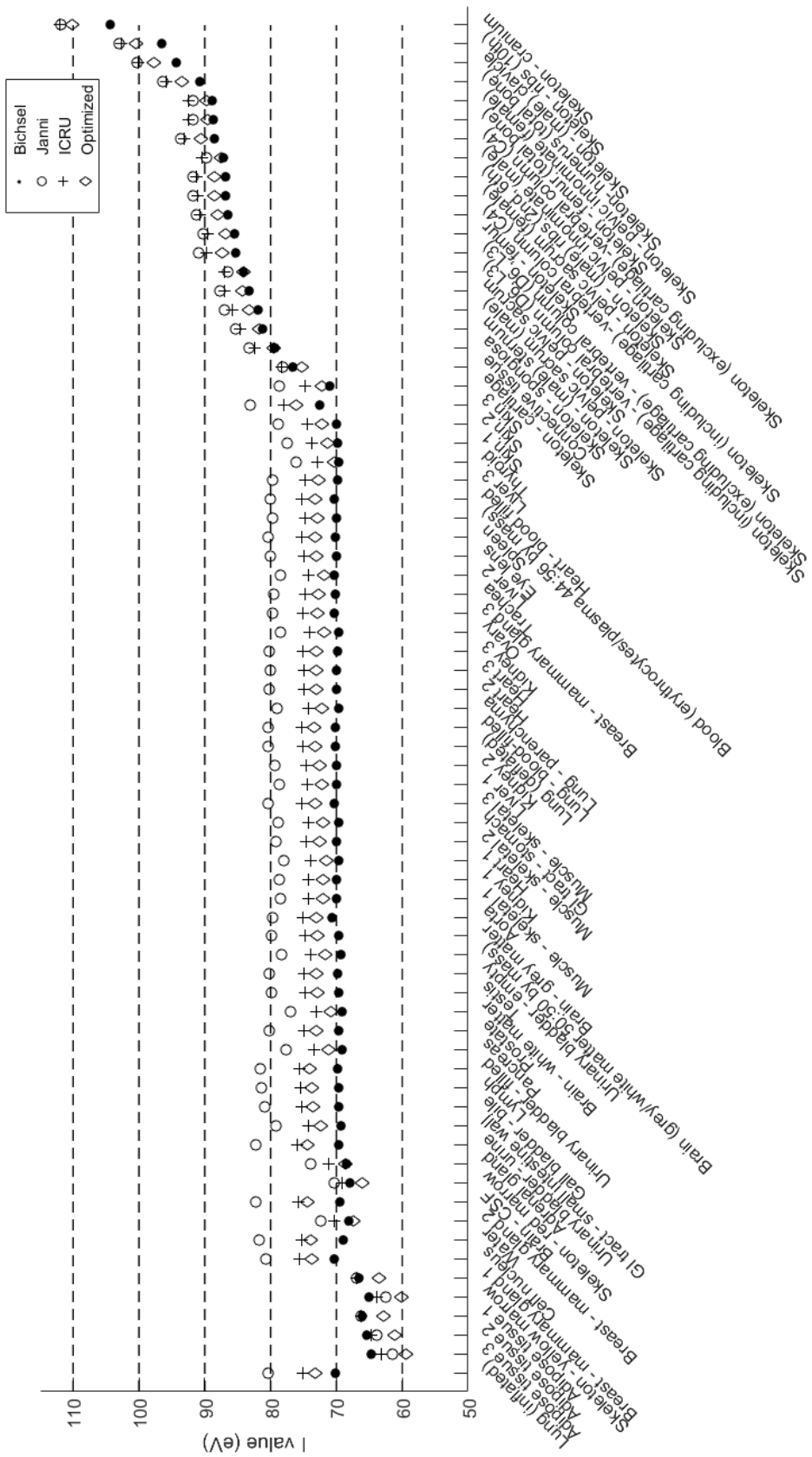

Figure 3. Human tissue I-values using optimized and literature elemental I-values.

The aim of this work is to assess the errors in using the current schemes available for computing the RSP. As such, the RSP differences when using the Bichsel, Janni and ICRU approaches were compared to those values obtained when using optimized elemental I-values with the Schneider approximation (equation 8). The impact of not using optimized elemental I-values to match measurement data can be seen in figure 4, by computing the errors for each approach across 72 human tissues.

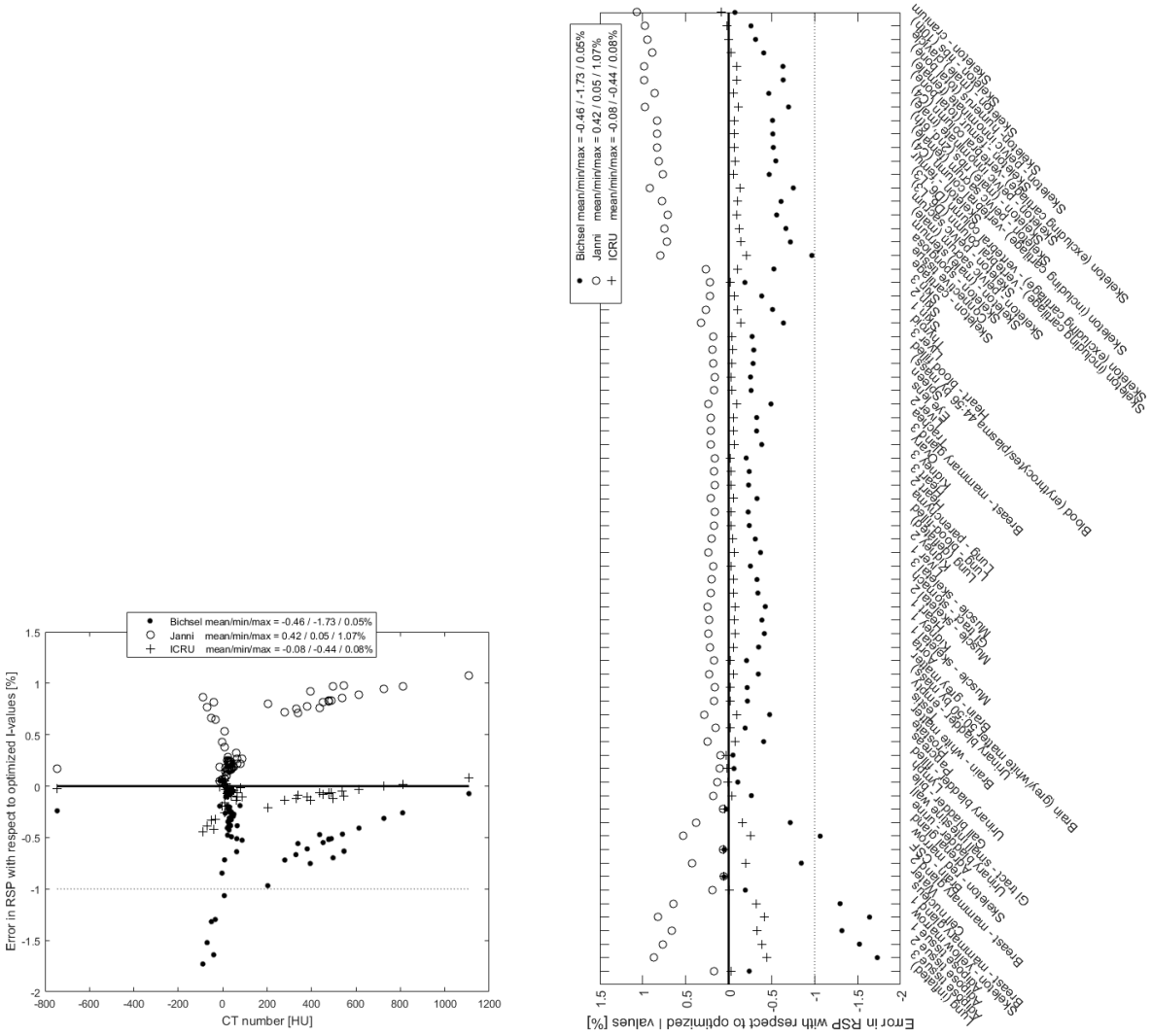

Figure 4. Errors in the RSP for 72 human tissues, calculated using literature elemental I-values compared to using the optimized I-values. Plotted against CT number (left); plotted as a list (right).

4. Discussion

Bethe-Bloch theory is widely used in proton therapy to compute the stopping power of tissue. The framework is known to have errors below 1 MeV (Emfietzoglou *et al* 2009), however the impact on the clinical range, which is of particular concern for this work, is negligible. Currently in literature there exist a number of different methods for computing the stopping power of tissue, with no clear consensus as to which approach is the most accurate. The absolute stopping power can be computed using the Bichsel, Janni and ICRU formulae (equations 3, 5 and 7), while the RSP can be computed directly using the Schneider approximation (equation 8). Due to its ease of use, the Schneider approximation and its variants such as de Kock are most commonly used. However, the user is required to select a set of I-values and the impact of using different datasets is not clear.

With no clarity on which approach is the most accurate, comparison was made with measurements of Gammex tissue substitutes. Separate Bragg peak shift measurements of a pencil proton beam were made with a Markus parallel plate ionisation chamber and with the Zebra (Ion Beam Applications, Louvain-la-Neuve) and the RSP of each tissue substitute was measured. These were compared to theoretical RSP values computed with the absolute stopping power methods (Bichsel, Janni and ICRU) and the Schneider RSP method with the three different I-value datasets.

4.1. Relative stopping power calculations

If calculated using the approach of first calculating the stopping power, this theoretical calculation of the RSP, one of the fundamental steps of the stoichiometric calibration procedure, has a RMSE/mean error of: +1.1/-0.1% for Bichsel (equation 3); +1.2/+0.7% for Janni (equation 5); and +1.3/-0.8% for ICRU (equation 7). If calculated using the Schneider approximation (equation 8), the RMSE/mean errors follow a similar trend: +1.9/-1.6% for Bichsel I-values; +1.1/+0.8% for Janni I-values; +0.9/-0.5% for ICRU I-values. Using the Bichsel absolute stopping power approach or using the Schneider approximation with the ICRU elemental I-values leads to the lowest errors.

It can be seen from inspection of tables 5 and 6 that these differences vary across the CT number range. The largest differences are typically found in the lower density lung inserts (underestimations

of more than 3%). Such RSP errors will translate into proton range errors and it has been shown that correct proton beam range prediction is particularly critical in regions such as the lung (Seco *et al* 2012).

4.2. How to correct the stoichiometric calibration

In an attempt to provide a solution to these discrepancies, an approach was developed in which the elemental I-values were optimized to fit to measurement data. As the Schneider RSP formula is the most common approach (for convenience) and the ICRU dataset is the most recently published set of I-values, with the best fit to measurements, these were used as the starting point for the optimization. The I-values of only 7 of the 15 elements were allowed to vary in the optimization procedure, and only by modest amounts according to the uncertainties in ICRU Report 49. Despite these restrictions, it was still possible to reduce the RMSE in the tissue insert RSP from 0.96% to 0.76% and the mean error significantly. The authors are confident that allowing a more relaxed I-value variation during the optimization would lead to further reductions in RSP errors; however it is important the I-values remain within typical physical limits. More relaxed constraints in the optimisation could be justified if one compares with the Bichsel and Janni I-values in table 1. Compared to the ICRU I-values, the Bichsel and Janni I-values have mean/max differences of -5.7/-12.1% and -4.1/+19.3%, respectively, which are considerably larger than the mean/max (1.5/8.4%) uncertainties that were allowed in the optimisation. Additionally, the optimizer is flexible and any measurements with larger uncertainties can be removed from the optimization process (e.g. lung inserts), if not considered reliable.

To assess the potential impact of using the Bichsel, Janni and ICRU I-values on proton therapy patients, comparisons were made with the optimized ICRU I-values across a range of human tissues. Figure 4 shows that mean/max differences across 72 human tissues were: -0.5%/-1.7% for Bichsel; +0.4%/+1.1% for Janni; and -0.1%/-0.4% for ICRU I-values. Although the mean differences are small (to be expected from only allowing minor variations in I-values), larger differences could be found in the bony and fatty regions (+1.1 for Janni in the Skeleton Cranium, -1.7% for Bichsel in Adipose Tissue 3, for example), which could be a concern for particular treatment sites. As such, we suggest

that an additional step should be added to the stoichiometric calibration procedure, in which RSP values are fitted to measurement through the optimization of elemental I-values. These I-values should be used in subsequent estimates of human tissue RSPs, which are used to form the stoichiometric calibration curve.

5. Conclusion

There are four clear methods for calculating the RSP of a given tissue. Three involve the computation of the stopping power of the tissue, which must then be divided by the respective stopping power of water over the same energy range (Bichsel 1972, Janni 1982, ICRU 1993). To account for the different formulae and corrections, each source has its own set of I-values. Comparing the RSPs of Gammex inserts determined using a simple Bragg peak shift measurement in a proton beam, it was found that the Bichsel approach leads to a small mean underestimation in the RSP (-0.1%); the Janni approach leads to a mean overestimation (+0.7%); while the ICRU also underestimates (-0.8%). The fourth method is an approximation in which the RSP is computed directly (Schneider *et al* 1996), using any set of I-values. The mean errors for this approach were generally higher in magnitude and the ICRU I-values showed the best match.

Using the Schneider approximation, the ICRU elemental I-values were optimized until the theoretical tissue substitute RSP values matched measurements (mean error reduced from -0.53% to +0.11%). The impact of not using these optimized elemental I-values was assessed by calculating the RSP of 72 human tissues with the Bichsel, Janni and ICRU elemental I-values. It was shown that failing to use optimized I-values could introduce errors of up to -1.7%/+1.1%/-0.4% for Bichsel/Janni/ICRU respectively. As such, we propose that an additional step should be added to the current stoichiometric calibration procedure that involves actual measurement of the tissue insert RSPs in a proton beam. Elemental I-values should then be optimized to match these measurements and these values should be

used in step four of the current stoichiometric procedure, the theoretical calculation of the RSP of human tissues.

6. Acknowledgements

This project was funded equally by the Engineering and Physical Sciences Research Council (UK) and Ion Beam Applications (Louvain-La-Neuve, Belgium). We would like to acknowledge the support of Dr Hsiao-Ming Lu of Massachusetts General Hospital, for his help in facilitating the project. We would also like to acknowledge Paige Taylor from IROC Houston, who provided information of the current use of the stoichiometric calibration.

7. References

Ainsley C G and Yeager C M 2014 Practical considerations in the calibration of CT scanners for proton therapy. *J. Appl. Clin. Med. Phys.* **15** 4721 Online: http://www.ncbi.nlm.nih.gov/pubmed/24892347

Andreo P 2009 On the clinical spatial resolution achievable with protons and heavier charged particle radiotherapy beams. *Phys. Med. Biol.* **54** N205–15 Online: http://www.ncbi.nlm.nih.gov/pubmed/19436099

Arbor N, Dauvergne D, Dedes G, Létang J M, Parodi K, Quiñones C T, Testa E and Rit S 2015 Monte Carlo comparison of x-ray and proton CT for range calculations of proton therapy beams *Phys. Med. Biol.* **60** 7585–99 Online: http://stacks.iop.org/0031-9155/60/i=19/a=7585?key=crossref.57a1486c25f9eea1404e24c3be3deb7c

Bichsel H 1972 Passage of charged particles through matter *American Institute of Physics Handbook* ed E D Gray (New York: McGraw-Hill)

Bichsel H and Hiraoka T 1992 Energy loss of 70 MeV protons in elements *Nucl. Instruments Methods Phys. Res. Sect. B Beam Interact. with Mater. Atoms* **66** 345–51 Online: http://linkinghub.elsevier.com/retrieve/pii/0168583X92959954

Chvetsov A V and Paige S L 2010 The influence of CT image noise on proton range calculation in radiotherapy planning. *Phys. Med. Biol.* **55** N141–9

Cormack A 1963 Representation of a Function by Its Line Integrals, with Some Radiological Applications *J. Appl. Phys.* **34** 2722–7 Online: http://link.aip.org/link/JAPIAU/v34/i9/p2722/s1&Agg=doi

Doolan P J, Testa M, Sharp G, Bentefour E H, Royle G and Lu H-M 2015 Patient-specific stopping power calibration for proton therapy planning based on single-detector proton radiography *Phys. Med. Biol.* **60** 1901–17

Emfietzoglou D, Garcia-Molina R, Kyriakou I, Abril I and Nikjoo H 2009 A dielectric

response study of the electronic stopping power of liquid water for energetic protons and a new I-value for water. *Phys. Med. Biol.* **54** 3451–72 Online: http://www.ncbi.nlm.nih.gov/pubmed/19436107

Esposito M, Anaxagoras T, Evans P M, Green S, Manolopoulos S, Nieto-Camero J, Parker D J, Poludniowski G, Price T, Waltham C and Allinson N M 2015 CMOS Active Pixel Sensors as energy-range detectors for proton Computed Tomography *J. Instrum.* **10** C06001–C06001 Online: http://stacks.iop.org/1748-0221/10/i=06/a=C06001?key=crossref.2b994d3e8ac4b2ad7c19aded6bb0f96c

Gottschalk B 2003 On the Characterization of Spread-Out Bragg Peaks and the Definition of "Depth" and "Modulation" 1–23 Online: http://huhelp.harvard.edu/~gottschalk/BGdocs.zip/SOBP.pdf

Hanson K, Bradbury J, Cannon T, Hutson R, Laubacher D, Macek R, Paciotti M and Taylor C 1981 Computed tomography using proton energy loss. *Phys. Med. Biol.* **26** 965–83 Online: http://www.ncbi.nlm.nih.gov/pubmed/6275424

Hurley R F, Schulte R W, Bashkirov V A, Wroe A J, Ghebremedhin A, Sadrozinski H F-W, Rykalin V, Coutrakon G, Koss P and Patyal B 2012 Water-equivalent path length calibration of a prototype proton CT scanner. *Med. Phys.* **39** 2438–46 Online: http://www.ncbi.nlm.nih.gov/pubmed/22559614

ICRU 1989 International Commission on Radiation Units and Measurements Report 44: Tissue substitutes on radiation units and measurement

ICRU 1992 International Commission on Radiation Units and Measurements Report 46: Photon, electron, proton and neutron interaction data for body tissues *Rep. 46*

ICRU 1993 International Commission on Radiation Units and Measurements Report 49: Stopping powers and ranges for protons and alpha particles

Ion Beam Applications *User Manual: Zebra with OmniPro-Incline*

Janni F 1982 Part 1 - Proton range-energy tables, 1 keV-10 GeV. Energy loss, range, path length, time-of-flight, straggling, multiple scattering and nuclear interaction probability *At. Data Nucl. Data Tables* **27** 147–339

Kanematsu N, Matsufuji N, Kohno R, Minohara S and Kanai T 2003 A CT calibration method based on the polybinary tissue model for radiotherapy treatment planning *Phys. Med. Biol.* **48** 1053–64

de Kock E A 2003 *Program CT CALIBRATE: CT calibration curves for proton radiotherapy planning*

Lagarias J, Reeds J, Wright M and Wright P 1998 Convergence properties of the nelder-mead simplex method in low dimensions *SIAM J. Optim.* **9** 112–47 Online: http://epubs.siam.org/doi/abs/10.1137/S1052623496303470

Liamsuwan T, Uehara S, Emfietzoglou D and Nikjoo H 2011 Physical and biophysical properties of proton tracks of energies 1 keV to 300 MeV in water. *Int. J. Radiat. Biol.* **87** 141–60

Liamsuwan T, Uehara S and Nikjoo H 2015 Microdosimetry of the Full Slowing Down of

Protons Using Monte Carlo Track Structure Simulations *Radiat. Prot. Dosimetry* **166** 1–5 Online: http://rpd.oxfordjournals.org/cgi/doi/10.1093/rpd/ncv204

Ödén J, Zimmerman J, Bujila R, Nowik P and Poludniowski G 2015 Technical Note: On the calculation of stopping-power ratio for stoichiometric calibration in proton therapy *Med. Phys.* **42** 5252–7 Online: http://scitation.aip.org/content/aapm/journal/medphys/42/9/10.1118/1.4928399

Paganetti H 2012 Range uncertainties in proton therapy and the role of Monte Carlo simulations *Phys. Med. Biol.* **57** R99–117 Online: http://stacks.iop.org/0031-9155/57/i=11/a=R99?key=crossref.4b6c83cb5125b4a360ead936994fceb4

Qi Z-Y, Huang S-M and Deng X-W 2006 Calibration of CT values used for radiation treatment planning and its impact factors *Chin. J. Cancer* **25** 110–4

Sadrozinski H 2003 Issues in Proton Computed Tomography *Nucl. Instruments Methods Phys. Res. Sect. A Accel. Spectrometers, Detect. Assoc. Equip.* **511** 275–81 Online: http://linkinghub.elsevier.com/retrieve/pii/S0168900203018060

Sánchez-Parcerisa D, Gemmel a, Jäkel O, Parodi K and Rietzel E 2012 Experimental study of the water-to-air stopping power ratio of monoenergetic carbon ion beams for particle therapy. *Phys. Med. Biol.* **57** 3629–41 Online: http://www.ncbi.nlm.nih.gov/pubmed/22596046

Schaffner B and Pedroni E 1998 The precision of proton range calculations in proton radiotherapy treatment planning: experimental verification of the relation between CT-HU and proton stopping power *Phys. Med. Biol.* **43** 1579–92

Schneider U and Pedroni E 1995 Proton radiography as a tool for quality control in proton therapy *Med. Phys.* **22** 353–63

Schneider U, Pedroni E and Lomax A 1996 The calibration of CT Hounsfield units for radiotherapy treatment planning *Phys. Med. Biol.* **41** 111–24 Online: http://stacks.iop.org/0031-9155/41/i=1/a=009?key=crossref.7cef62664dbeba7f6a11f0639b13a9e8

Schneider U, Pemler P, Besserer J, Pedroni E, Lomax A and Kaser-Hotz B 2005 Patient specific optimization of the relation between CT-Hounsfield units and proton stopping power with proton radiography *Med. Phys.* **32** 195–9 Online: http://link.aip.org/link/MPHYA6/v32/i1/p195/s1&Agg=doi

Schneider W, Bortfeld T and Schlegel W 2000 Correlation between CT numbers and tissue parameters needed for Monte Carlo simulations of clinical dose distributions *Phys. Med. Biol.* **45** 459–78 Online: http://iopscience.iop.org/0031-9155/45/2/314

Schulte R, Bashkirov V, Loss Klock M, Li T, Wroe A, Evseev I, Williams D and Satogata T 2005 Density resolution of proton computed tomography *Med. Phys.* **32** 1035–46 Online: http://link.aip.org/link/MPHYA6/v32/i4/p1035/s1&Agg=doi

Schulte R, Bashkirov V, Mueller K, Heimann J, Johnson L, Keeney B, Sadrozinski H, Seiden A, Williams D, Peggs S, Satogata T and Woody C 2004 Conceptual design of a proton computed tomography system for applications in proton radiation therapy *IEEE Trans. Nucl. Sci.* **51** 866–72 Online:

http://ieeexplore.ieee.org/lpdocs/epic03/wrapper.htm?arnumber=1311983

Seco J, Panahandeh H R, Westover K, Adams J and Willers H 2012 Treatment of non-small cell lung cancer patients with proton beam-based stereotactic body radiotherapy: dosimetric comparison with photon plans highlights importance of range uncertainty. *Int. J. Radiat. Oncol. Biol. Phys.* **83** 354–61

Seltzer S and Berger M 1982 Evaluation of the collision stopping power of elements and compounds for electrons and positrons *Int. J. Appl. Radiat. Isot.* **33** 1189–218

Talamonti C, Reggioli V, Bruzzi M, Bucciolini M, Civinini C, Marrazzo L, Menichelli D, Pallotta S, Randazzo N and Sipala V 2010 Proton radiography for clinical applications *Nucl. Instruments Methods Phys. Res. Sect. A Accel. Spectrometers, Detect. Assoc. Equip.* **612** 571–5 Online: http://linkinghub.elsevier.com/retrieve/pii/S0168900209015915

Taylor P 2015a IROC Houston, Private Communication

Taylor P 2015b IROC Houston's Proton Beam Validation for Clinical Trials *AAPM 57th Meeting*

Testa M, Verburg J M, Rose M, Min C H, Tang S, Bentefour E H, Paganetti H and Lu H-M 2013 Proton radiography and proton computed tomography based on time-resolved dose measurements. *Phys. Med. Biol.* **58** 8215–33 Online: http://www.ncbi.nlm.nih.gov/pubmed/24200989

Verburg J M and Seco J 2012 CT metal artifact reduction method correcting for beam hardening and missing projections. *Phys. Med. Biol.* **57** 2803–18

White D, Woodard H and Hammond S 1987 Average soft-tissue and bone models for use in radiation dosimetry. *Br. J. Radiol.* **60** 907–13

Woodard H Q and White D R 1982 Bone models for use in radiotherapy dosimetry. *Br. J. Radiol.* **55** 277–82

Woodard H and White D 1986 The composition of body tissues *Br. J. Radiol.* **59** 1209–18

Yang M, Zhu X R, Park P C, Titt U, Mohan R, Virshup G, Clayton J E and Dong L 2012 Comprehensive analysis of proton range uncertainties related to patient stopping-power-ratio estimation using the stoichiometric calibration. *Phys. Med. Biol.* **57** 4095–115

Zhang R, Taddei P J, Fitzek M M and Newhauser W D 2010 Water equivalent thickness values of materials used in beams of protons, helium, carbon and iron ions *NIH Public Access* **55** 2481–93

Zygmanski P and Gall K 2000 The measurement of proton stopping power using proton-cone-beam computed tomography *Phys. Med. Biol.* **45** 511–28 Online: http://iopscience.iop.org/0031-9155/45/2/317